JACS
JOURNAL OF THE AMERICAN CHEMICAL SOCIETY

Article

Zinc Photocages with Improved Photophysical Properties and Cell Permeability Imparted by Ternary Complex Formation

Prem N. Basa, Chelsea A. Barr, Kady M Oakley, Xiaomeng Liang, and Shawn C Burdette

J. Am. Chem. Soc., **Just Accepted Manuscript** • DOI: 10.1021/jacs.9b05504 • Publication Date (Web): 30 Jun 2019

Zinc Photocages with Improved Photophysical Properties and Cell Permeability Imparted by Ternary Complex Formation

Prem N. Basa, Chelsea A. Barr, Kady M.Oakley, Xiaomeng Liang, and Shawn C. Burdette*

Department of Chemistry and Biochemistry, Worcester Polytechnic Institute,
100 Institute Road. Worcester, Massachusetts 01609-2280

ABSTRACT: Photocaged complexes can control the availability of metal ions to interrogate cellular signaling pathways. We describe the new photocage, {bis[(2-pyridyl)methyl]amino}(9-oxo-2-xanthenyl)acetic acid (XDPAdeCage, **1**), which utilizes a 2-xanthone acetic acid group to mediate a photodecarboxylation reaction. XDPAdeCage photolyzes with quantum yield of 27%, and binds Zn^{2+} with 4.6 pM affinity, which decreases by over 4 orders of magnitude after photolysis. For comparison to our previous approach to Zn^{2+} release via photodecarboxylation, the analogous photocage {bis[(2-pyridyl)methyl]amino}(m-nitrophenyl)acetic acid (DPAdeCage, **2**) which uses a *meta*-nitrobenzyl chromophore was also prepared and characterized. The advantages of the 2-xanthone acetic acid chromophore include red-shifted excitation and a higher extinction coefficient at the preferred uncaging wavelength. The neutral ternary complex of $[Zn(XDPAdeCage)]^+$ with the anionic ligand pyrithione is membrane permeable, which circumvents the need to utilize invasive techniques to introduce intracellular Zn^{2+} fluctuations. Using fluorescent imaging, we have confirmed transport of Zn^{2+} across membranes; in addition, RT-PCR experiments demonstrate changes in expression of Zn^{2+}-responsive proteins after photolysis.

INTRODUCTION

Efforts to interrogate Zn^{2+} signals have focused mostly on the development and application of fluorescent probes.[1] Improvements in probe selectivity, optical properties, and targeting strategies have facilitated testing Zn^{2+}-mediated neurotransmission.[2] With the exception of several ZP derivatives however,[3-7] most new probes seldom advance beyond proof-of-concept imaging. Recent studies have demonstrated that fluorescent probes can be powerful tools in unraveling signaling pathways; however, probes are limited to imaging Zn^{2+} released in response to stimulation. In the absence of known stimuli, Zn^{2+} signals could evade detection by fluorescence techniques. Tools capable of spatiotemporally controlled Zn^{2+} release allow interrogation of such pathways.[8]

Our group previously developed photocaged complexes for Zn^{2+} inspired by the *ortho*-nitrobenzyl systems for Ca^{2+}.[9] ZinCast photocages modulate concentrations by weakening a Zn^{2+}–anilino nitrogen interaction; however, these complexes cannot buffer Zn^{2+} at physiologically relevant concentrations.[10] In contrast, ZinCleav photocages bind with up to fM affinity, and exhibit a 10^8 decrease in Zn^{2+} binding strength (ΔK_d; ΔK_d = K_d photoproduct/K_d photocage) upon photolysis.[11-12] Despite coupling suitable Zn^{2+} buffering capacities with an effective uncaging strategy, the modest photolysis quantum yields of ZinCleav photocages ($\Phi_{photolysis}$ < 5%), coupled with UV excitation (λ_{max}) and low extinction coefficients (ε), present challenges in cells.

We recently described NTAdeCage based on the decarboxylation of a *m*-nitrophenylacetic acid (*m*NPA) derivative to start addressing some of these challenges (Figure 1).[13] While NTAdeCage exhibited a decrease in binding affinity (pM) and a modest ΔK_d (10^5), the $\Phi_{photolysis}$ improved by a factor of six (~30%). The synthesis of NTAdeCage is also more manageable compared than that of ZinCleav. Although NTAdeCage and ZinCleav uncage by different photochemical mechanisms, both utilize different isomers of nitrobenzyl chromophores that have λ_{max} below 300 nm and weak absorbance in the near-UV. Uncaging metal ions by breaking chemical bonds requires higher energy light when using single photon techniques; however, any adverse effects to cells from such irradiation can be limited by increasing the absorbance of light at standard instrumental uncaging wavelengths (ca. 350 nm).

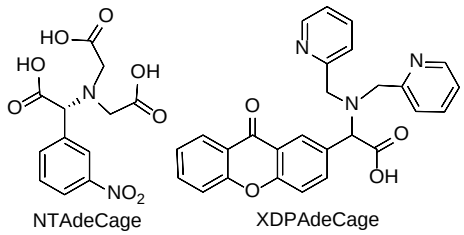

Figure 1. Structure of NTAdeCage based on a *m*-nitrophenyl acetic acid photocaging group, and XDPAdeCage that uses a xanthone acetic acid chromophore.

Based on the encouraging results with NTAdeCage, we sought to expand the scope of the photodecarboxylation strategy. In addition to suboptimal optical properties, metal ion exchange between $[Zn(NTAdeCage)]^{1-}$ and Ca^{2+} and Mg^{2+}, which are often present at much higher concentrations in cells, could obfuscate the source of any measured biological response. The use of $[Zn(NTAdeCage)]^{1-}$ also can be limited by localization in biological systems. Although we leveraged the charge on $[Zn(NTAdeCage)]^{1-}$ to prevent cellular uptake of the photocaged complex when investigating Zn^{2+} entry through protein importers,[13] interrogating intracellular signaling processes with this complex would be unfeasible without

invasive techniques to deliver the complex across cell membranes.

EXPERIMENTAL

General synthetic procedures. All materials were obtained in their highest pure form available from Fisher, Acros Organic or Alfa Aesar and used without further purification. Dichloroethane (DCE), dichloromethane (CH_2Cl_2), acetonitrile (CH_3CN) were purged with argon and dried using a Seca Solvent Purification System. All chromatography and thin-layer chromatography (TLC) were performed on silica gel (230-400 mesh) from Silicycle. TLCs were developed using mixtures of ether/hexanes (Et_2O), CH_2Cl_2/hexanes, ethyl acetate (EtOAc) /hexanes and CH_2Cl_2/methanol (CH_3OH) as specified and were visualized with 254 or 365 nm light or stained with iodine (I_2). ^1H and ^{13}C NMR were recorded using a 500 MHz Bruker-Biospin NMR instrument, and chemical shifts are reported in ppm on the δ scale relative to tetramethylsilane (TMS). FT-IR spectra were recorded using Bruker Optics Vertex 70 with MIR source as neat crystalline powdered samples and Spectrum 100 Version 10.4.2 (PerkinElmer) fitted with diamond ATR as oils. LC/MS was carried on a Single Quadruple, Agilent Technologies 1200 series LC system. High resolution mass spectra were obtained at the University of Notre Dame mass spectrometry facility using microTOF instrument operating in positive ionization mode (+ESI-TOF). Melting-point information was obtained using Hydrothermal Mel-Temp instrument. Xantone acetic acid ester (**3**, XAA-ester) was prepared as previously described.[14]

Methyl bromo(9-oxo-2-xanthenyl)acetate (4). XAA-ester (1.0 g, 3.7 mmol) was combined with *N*-bromosuccinimide (NBS, 0.98 g, 5.5 mmol) and 2,2'- azobisbutyronitrile (AIBN, 0.06 g, 0.37 mmol) in DCE (10 mL). The resulting mixture was refluxed for 3 h. DCE was removed under reduced pressure and the product was extracted into CH_2Cl_2 (2×50 mL), and the combined organic extracts were dried over Na_2SO_4. Solvent removal yielded a pale yellow semi-solid. Flash chromatography on silica using gradient elution (Et_2O/hexanes 1:1→Et_2O) yielded **4** as pale yellow crystalline solid (0.90 g, 73%). TLC (R_f = 0.5, silica, 1:1, ether/hexanes); mp = 120-122°C. ^1H NMR (500 MHz, $CDCl_3$/ TMS) δ 8.39 (s, 1 H), 8.34 (dd, *J* = 7.8, 1.5 Hz, 1 H), 8.06 (dd, *J* = 8.8, 2.4 Hz, 1 H), 7.75 (td, *J* = 7.8, 1.5 Hz, 1 H), 7.55 (d, *J* = 8.8 Hz, 1 H), 7.51 (d, *J* = 8.7 Hz, 1 H), 7.41 (td, *J* = 7.5, 0.9 Hz, 1 H), 5.50 (s, 1 H), 3.82 (s, 3 H). ^{13}C NMR (125 MHz) δ 176.7, 168.7, 156.5, 156.2, 135.5, 135.3, 131.8, 126.9, 124.5, 121.9, 126.9, 124.5, 121.9, 121.6, 119.3, 118.2, 53.7, 45.2. FT-IR (neat, cm^{-1}) 3044.5, 3004.6, 2947.2, 2325.3, 2161.4, 2051.6, 1980.0, 1738.9, 1653.8, 1610.7, 1592.3, 1488.5, 1474.8, 1465.1, 1435.5, 1363.9, 1339.8, 1326.0, 1315.6, 1269.8, 1233.4, 1216.2, 1191.5, 1176.5, 1162.4, 1145.9, 1121.9, 1109.8, 1008.9, 984.0, 926.9, 897.3, 883.8, 864.1, 839.8, 833.4, 807.7, 801.0, 788.9, 761.2, 753.9, 736.0, 724.5, 713.6, 705.1, 676.0, 660.2, 631.1, 603.7. HRMS (+ESI) calculated for ($C_{16}H_{12}BrO_4$) 346.9891, observed 346.9913.

Methyl {bis[(2-pyridyl)methyl]amino}(9-oxo-2-xanthenyl)acetate (5). Compound **4** (0.050 g, 0.14 mmol) was combined with potassium carbonate (K_2CO_3, 0.0172 g, 0.12 mmol), sodium iodide (0.0187 g, 0.12 mmol), and dipicolylamine (DPA, 0.025 g, 0.12 mmol) in CH_3CN (5 mL). After 18 h reaction at room temperature, the reaction mixture was diluted with H_2O (10 mL) and the product was extracted into CH_2Cl_2 (2×25 mL). The combined extracts were dried over Na_2SO_4. Solvent removal under reduced pressure yielded dark colored oil. Flash chromatography on alumina using gradient elution (Et_2O→CH_2Cl_2→CH_2Cl_2/CH_3OH, 9.5:0.5) yielded **5** as dark brown oil (0.030 g, 45%). TLC (R_f= 0.7, silica, 1:1, CH_2Cl_2/ CH_3OH).^1H NMR (500 MHz, $CDCl_3$/ TMS) δ 8.50 (dq, = 4.8, 1.2, 0.8 Hz, 2 H), 8.36 (d, = 2.4 Hz, 1 H), 8.33 (dd, = 4.7, 1.6 Hz, 1 H), 7.87 (dd, = 5.5, 2.2 Hz, 1 H), 7.73 (td, = 8.8, 1.5 Hz, 1 H), 7.64 (td, = 8.6, 1.7 Hz, 2 H), 7.51- 7.48 (m, 4 H), 7.38 (td, = 8.0, 0.9 Hz, 1 H), 7.12 (td, = 6.7, 1.1 Hz, 2 H), 4.88 (s, 1 H), 4.08 (d, = 14.5 Hz, 2 H), 3.92 (d, =14.6 Hz, 2 H), 3.79 (s, 3 H). ^{13}C NMR (125 MHz) δ 177.0, 172.1, 159.3, 156.0, 149.0, 137.0, 135.8, 135.1, 132.5, 127.1, 126.9, 124.3, 123.3, 122.4, 122.0, 121.7, 118.6, 118.2, 67.3, 56.9, 52.2. FT-IR (neat, cm^{-1}) 1734.4, 1657.0, 1652.4, 1616.6, 1609.3, 1589.9, 1488.1, 1464.4, 1432.8, 1322.6, 1233.3, 1207.9, 1143.1, 1108.9, 1092.0, 1046.8, 995.2, 882.5, 827.8, 756.1, 725.1, 682.2. HRMS (+ESI) calculated for ($C_{28}H_{24}N_3O_4$) 466.1733, observed 466.1761.

{Bis[(2-pyridyl)methyl]amino}(9-oxo-2-xanthenyl)acetic acid (XDPAdeCage, 1). Compound **5** (0.15 g, 0.43 mmol) was dissolved in CH_3OH (5 mL) and NaOH (0.17 g, 4.3 mmol) was added in small portions. Water (0.5 mL) was added and the reaction mixture was stirred at room temperature for 18 h. After removing CH_3OH under reduced pressure, 1 g of crushed ice was added to the resulting semi-solid material. After adjusting the pH to 6 using HCl, the product was extracted into EtOAc (2×10 mL). The combined extracts were dried over Na_2SO_4. Solvent removal under reduced pressure yielded **5** as a pale brown solid (0.10 g, 69%). TLC (R_f = 0.2, silica, 9:1, CH_2Cl_2/CH_3OH); mp = 170-172 °C. ^1H NMR (500 MHz, D_2O) δ 8.11 (d, *J* = 4.4 Hz, 1 H), 7.94 (s, 1 H), 7.75 (dd, *J* = 9.0, 1.6 Hz, 1 H), 7.49 (td, *J* = 7.7, 1.2 Hz, 2 H), 7.42 (d, *J* = 7.3 Hz, 1 H), 7.33 (d, *J* =7.8 Hz, 2 H), 7.19 (t, *J* = 7.4 Hz, 1 H), 6.99 (t, *J* = 6.1 Hz, 2 H), 6.84 – 6.79 (m, 2 H), 6.66 (d, *J* = 8.4 Hz, 1 H), 4.40 (s, 1 H), 3.79 (dd, *J* = 16.8, 4.4 Hz, 4 H) ^{13}C NMR (125 MHz) δ 177.4, 156.0, 154.7, 154.6, 145.2, 140.2, 135.9, 135.4, 134.0, 125.6, 125.0, 124.5, 123.9, 123.6, 119.7, 119.5, 118.2, 117.2, 73.7, 56.7. FT-IR (neat, cm^{-1}) 3063.9, 2837.6, 2325.3, 2161.3, 2051.5, 1979.9, 1706.8, 1656.9, 1610.8, 1592.7, 1570.4, 1489.3, 1464.9, 1434.9, 1368.3, 1349.9, 1322.4, 1269.8, 1221.2, 1140.8, 1123.6, 1095.2, 1051.0, 1019.6, 995.7, 976.1, 964.7, 916.6, 901.3, 883.3, 842.9, 820.5, 762.8, 733.0, 724.6, 682.2, 660.7, 644.6, 632.4, 610.4. HRMS (+ESI) calculated for ($C_{27}H_{22}N_3O_4$), 452.1605 and observed 452.1604.

Methyl {bis[(2-pyridyl)methyl]amino}phenylacetate (7). Methyl (2S) aminophenyl ethanoate (**6**, 2.03 g, 12.0 mmol) was combined with pyridine-2-carboxaldehyde (2.94 g, 27.0 mmol) in DCE (50 mL). $NaBH(O_2CH_3)_3$ (5.60 mg, 24.4 mmol) was added in small portions. After 24 h reaction at room temperature, the reaction mixture was diluted with saturated $NaHCO_3$ (20 mL). The product was extracted into CH_2Cl_2 (3×25 mL). The combined extracts were dried over Na_2SO_4. Solvent removal under reduced pressure yielded brown oil. Flash chromatography on silica using gradient elution (Et_2O→CH_2Cl_2) yielded **7** as white solid (1.25 g, 29.3%). TLC (R_f = 0.5, silica, 9:1, CH_2Cl_2/CH_3OH); mp= 67–69°C. ^1H NMR (500 MHz, $CDCl_3$) δ 8.49 (d, *J* = 4.9 Hz, 2 H), 7.62 (td, *J* = 7.6, 1.8 Hz, 2 H), 7.50 (d, *J* = 7.9 Hz, 2 H), 7.41 – 7.39 (m, 2 H), 7.36 – 7.32 (m, 2 H), 7.31 – 7.27 (m, 1 H),7.11 (t, J = 6.7 Hz, 2 H), 4.74 (s, 1 H), 4.07 (d, *J* = 14.5 Hz, 2 H), 3.89 (d, *J* = 15.2 Hz, 2 H), 3.75 (s, 3 H).^{13}C NMR (125 MHz, $CDCl_3$) δ 172.7, 160.0, 149.1, 136.5, 136.2, 129.1, 128.6, 128.2, 123.1, 122.1, 67.6, 57.0, 51.9. FT-IR (neat, cm^{-1}) 3062.0, 3011.2, 2950.4, 2906.5, 2854.9, 2325.4, 2161.2, 2051.5, 1975.2, 1732.9, 1590.0, 1570.6, 1495.5, 1473.5,

1445.5, 1431.1, 1371.4, 1351.5, 1206.4, 1278.5, 1247.1, 1206.8, 1185.7, 1173.7, 1136.0, 1089.0, 1078.1, 1048.6, 1032.1, 996.0, 981.0, 958.6, 913.6, 902.4, 820.8, 760.2, 699.0, 647.3, 619.2. HRMS (+ESI) calculated for ($C_{21}H_{22}N_3O_2$) 348.1693, observed 348.1706.

{Bis[(2-pyridyl)methyl]amino}phenylacetic acid (8). Compound **7** (900 mg, 2.6 mmol) was dissolved in CH_3OH (40 mL) and H_2O (1 mL) was mixed with NaOH (2.07 g, 51.8 mmol) in small portions. After 36 h reaction at room temperature, the solution was adjusted to pH 6.0 (6 M HCl, 7 mL). CH_3OH was removed under reduced pressure and the product was extracted into CH_2Cl_2 (3×25 mL). The combined extracts were dried over anhydrous Na_2SO_4. Solvent removal under reduced pressure yielded **8** as white powder (450 mg, 52%). TLC (R_f = 0.6, silica, 9:1, CH_2Cl_2/CH_3OH); mp= 97– 99°C. ^{1}H NMR (500 MHz, $CDCl_3$) δ 8.58 (d, *J* = 4.9 Hz, 2 H), 7.57 (td, *J* = 8.5, 1.7 Hz, 2 H), 7.34 – 7.28 (m, 5 H), 7.18 – 7.16 (m, 2 H), 7.14 – 7.12 (d, *J* = 7.7 Hz, 2 H), 4.87 (s, 1 H), 3.97 (d, *J* = 15.2 Hz, 2 H), 3.80 (d, *J* = 15.4 Hz, 2 H). ^{13}C NMR (125 MHz, $CDCl_3$) δ 174.5, 158.8, 148.7, 137.3, 135.6, 129.7, 128.8, 128.4, 123.1, 122.7, 70.4, 56.9. FT-IR (neat, cm^{-1}) 3061.1, 2843.2, 2325.3, 2161.3, 2051.5, 1980.0, 1700.9, 1592.2, 1570.5, 1494.6, 1474.5, 1434.8, 1367.9, 1223.5, 1185.4, 1143.0, 1094.7, 1049.5, 1031.2, 1019.7, 1002.8, 995.1, 977.4, 902.4, 838.7, 762.4, 700.1, 667.4, 638.9, 617.0. HRMS (+ESI) calculated for ($C_{20}H_{20}N_3O$) 334.1571, observed 334.1550.

{Bis[(2-pyridyl)methyl]amino}(*m*-nitrophenyl)acetic acid (DPAdeCage, 2). Compound **8** (102 mg, 0.306 mmol) was cooled with in an ice/salt bath and concentrated H_2SO_4 (1.0 mL) was added. After the solids dissolved, nitric acid (69-70% HNO_3, 0.18 mL, 3.0 mmol) was added and the reaction mixture was stirred in the dark at 0 °C for 1 h. Crushed ice was added to the reaction and the excess acid was neutralized with $NaHCO_3$. The product was extracted into EtOAc (2×25 ml), the combined extracts were washed with saturated NaCl and dried over Na_2SO_4. Solvent removal yielded a light-brown semi-solid (96 mg, 70% yield). TLC (R_f = 0.8, silica, 9:1, CH_2Cl_2/CH_3OH); mp = 118-120 °C. ^{1}H NMR (500 MHz, D6-DMSO) δ 8.49 (s, 2 H), 8.25 – 8.13 (m, 2 H), 7.88 (d, *J* = 7.85 Hz, 1 H), 7.77 – 7.63 (m, 3 H), 7.47 – 7.44 (m, 2 H), 7.26 (s, 1 H), 4.83 (s, 1 H), 4.01 (d, *J* = 18.4 Hz, 2 H), 3.88 – 3.83 (d, 2 H). ^{13}C NMR (125 MHz, $CDCl_3$) δ 192.3, 172.1, 159.0, 148.8, 147.6, 136.6, 130.6, 129.6, 124.3, 122.7, 122.5, 122.2, 122.1, 122.0, 110.9, 108.7, 56.4, 53.5. FT-IR (neat, cm^{-1}) 3068.9, 2923.4, 2856.6, 2455.4, 2365.5, 1980.9, 1718.7, 1597.6, 1570.1, 1524.0, 1475.3, 1433.2, 1344.5, 1278.7, 1227.7, 1193.3, 1139.2, 1085.7, 1053.7, 1014.9, 981.0, 959.3, 899.1, 852.7, 768.7, 692.0, 640.6. HRMS (+ESI) calculated for ($C_{20}H_{19}N_4O_4$) 379.1400, observed 379.1428.

[Zn(8)]Cl. A 0.5 ml solution of compound **8** (0.1 M, 0.05 mmol) was mixed with 0.5 mL of $ZnCl_2$ (0.1 M, 0.05 mmol) and 0.05 mL of pyridine in CH_3OH (1 M, 0.05 mmol), and sonicated for 5 min. After cooling for 36 h at 5 °C **[Zn(8)]Cl** precipitated as yellow blocks suitable for X-ray crystallographic analysis (10 mg, 46% yield). Mp = >260 °C. ^{1}H NMR (500 MHz, CD_3CN) δ 9.08 (d, *J* = 4.9 Hz, 1 H), 8.98 (d, *J* = 5.3 Hz, 1 H), 8.05 (t, *J*= 7.6 Hz, 1 H), 7.86 (t, *J* = 7.8 Hz, 1 H), 7.62 (t, *J* = 6.7 Hz, 1 H), 7.56 – 7.49 (m, 2 H), 7.33 – 7.30 (m, 3 H), 7.28 – 7.24 (m, 2 H), 7.16 (d, *J* = 7.8 Hz, 1 H), 4.25 (d, *J* = 16.0 Hz, 1 H), 4.25 (s, 1 H), 4.07 (d, *J* = 16.0 Hz, 1 H), 3.80 (d, *J* = 16.6 Hz, 1 H), 3.58 (d, *J* = 16.5 Hz, 1 H). ^{13}C NMR (125 MHz, CD_3CN) δ 173.0, 156.4, 156.0, 149.6, 149.0, 141.7, 141.3, 135.0, 131.7, 128.6, 128.5, 125.4, 125.1, 124.6, 70.9, 56.0, 54.5. FT-IR (neat, cm^{-1}) 3085.2, 3019.7, 2932.0, 2900.3, 2855.6, 2325.4, 2161.4, 2051.5, 1980.0, 1657.3, 1609.1, 1574.9, 1480.7, 1444.7, 1436.3, 1367.5, 1362.4, 1349.7, 1336.5, 1321.5, 1311.3, 1291.0, 1248.1, 1221.4, 1161.6, 1151.5, 1132.5, 1114.7, 1102.4, 1073.4, 1056.1, 1050.9, 1025.6, 1003.5, 995.4, 980.3, 944.2, 922.5, 897.4, 879.2, 870.2, 831.8, 791.3, 766.7, 748.6, 739.9, 728.6, 710.2, 667.8, 647.7, 637.7, 616.4. HRMS (+ESI) calculated for ($C_{20}H_{19}ClN_3O_2Zn$) 432.0436, observed 432.0451.

Collection and Reduction of X-ray Data. Structural analysis was carried out in the X-Ray Crystallographic Facility at Worcester Polytechnic Institute. Crystals were glued on tip of a glass fiber or were covered in PARATONE oil on 100 μm MiTeGen polyimide micromounts and were mounted on a Bruker-AXS APEX CCD diffractometer equipped with an LT-II low temperature device. Diffraction data were collected at room temperature or at 100(2) K using graphite monochromated Mo−Kα radiation (λ = 0.71073 Å) using the omega scan technique. Empirical absorption corrections were applied using the SADABS program.[15] The unit cells and space groups were determined using the SAINT+ program.[16] The structures were solved by direct methods and refined by full matrix least-squares using the SHELXTL program.[17] Refinement was based on F^2 using all reflections. All non-hydrogen atoms were refined anisotropically. Hydrogen atoms on carbon atoms were all located in the difference maps and subsequently placed at idealized positions and given isotropic U values 1.2 times that of the carbon atom to which they were bonded. Hydrogen atoms bonded to oxygen atoms were located and refined with isotropic thermal parameters. Mercury 3.1 software was used to examine the molecular structure. Relevant crystallographic information is summarized in Table 1, and selected bond distances and angles are provided in Tables 2. Additional X-ray data tables (Tables S2-S5) and fully labeled structure (Figure S52) can be found in the supporting information.

General spectroscopic methods. All aqueous solutions were prepared from Millipore (Biopak™ Ultrafiltration Cartridge) water. All organic solutions were prepared using spectroscopic grade solvents. HEPES (4-(2-hydroxyethyl)-1-piperizineethanesulfonic acid), TRIS HCl (tris(hydroxymethyl)aminomethane, THAM) and potassium chloride (KCl, 99.8%) were obtained from Fisher Scientific, and used without purification. The pHs of buffered solutions were measured using Acumet pH and the glass electrode was calibrated before each use. Stock solutions of metal salt solution were prepared using Millipore water. Zn^{2+} stock solution (9.02 mM) was prepared either from $ZnCl_2$ or $Zn(NO_3)_2{\cdot}4H_2O$ and calibrated using terpyridine.[18] Stock solution of Ca^{2+} was prepared from the perchlorate salt. HPLC grade CH_3CN, CH_3OH and DMSO were routinely used as co-solvents for preparing the stock solutions of ligands. UV-vis absorption spectra were obtained by taking sample solutions in 1.0 cm quartz cuvette at 25 ˚C with total volumes kept at 2 or 3.0 mL and recorded on Thermo Scientific Evolution 300 UV-vis spectrometer with inbuilt Cary winUV software controlled by Intel-Core2-Duo based PC. Fluorescence spectra were recorded on a Hitachi F-4500 spectrometer controlled by Pentium-IV PC run by FL solutions 2.0 software package. The excitation source was 150 W Xe arc lamp (Ushio Inc.) operating at a current rate of 5 A and equipped with photomultiplier tube with a power of 700 V. Spectra were routinely obtained by taking 2.0 or 3.0 mL sample solutions in 1.0 cm path length quartz cuvettes, acquired at 25 ˚C using 5 nm slit width.

Photolysis was carried at 25 ˚C in 1.0 cm quartz cuvette illuminated by 200 mW LED (Mouser Electronics, 365 nm) powered by a 700 Ma LuxDrive FlexBox using a variable DC source set at 12 VDC. Rate of photolysis and photoproducts were analyzed using LC/MS (Single Quadrupole, Agilent Technologies) by monitoring at changes at 254 nm. Routine quantum yield and metal binding assay methodologies, and the corresponding figures (Figures S17-S18 and S29), including competitive metal ion binding with Ca^{2+} and Mg^{2+} (Figures S21, S22 and S30) and photolysis experiments with pyrithione (S19, S20, S28 & S31) are located in the supporting information.

Determination of photoproducts using HPLC analysis. In a typical procedure, 3.0 mL of 1.0 mM stock solution (pH 7.5, 50% CH_3CN) of XDPAdeCage or $[Zn(XDPAdeCage)]^{1+}$ was photolyzed using irradiation for 60 s (365 nm, 200 mW). Similarly, fresh 3.0 mL solutions were subjected to 90 s and 180 s or irradiation. To 1.0 mL of the irradiated sample solutions were diluted with 25 µL aliquot of isonicotinic acid, as internal standard (0.2 M in CH_3OH, 0.1% HCl). The sample solutions were then subjected to LC-MS analysis. The uncaging of XDPAdeCage, $[Zn(XDPAdeCage)]^{1+}$ and the formation of photoproducts were confirmed using HPLC analysis. All the samples were eluted using an isocratic mixture of 95:5 CH_3CN:H_2O containing 0.1% formic acid at a flow rate of 0.3 mL/min. The chromatograms were recorded by monitoring the absorbance at 254 nm. The compounds corresponding to the individual peaks labeled in the HPLC traces (Figures 3 and 5) were identified by m/z values from the mass spectrum (Scheme 2). Additional HPLC traces recorded in different solvent systems (Figures S1-S7 and S23) and photoproduct formation pathways (Scheme S1-S2) can be found in the supporting information.

Cell Culturing and Imaging. Human dermal fibroblast cells (HDF) were plated onto sterilized 60×15 mm culture dishes and grown to ~60–80% confluency at 37 °C under an atmosphere of 5% CO_2. The media used to grow these cells was DMEM: F12 supplemented with 10% fetal bovine serum, 1% penicillin and streptomycin, and 1% non-essential amino acids. Zinpyr-1 labeling was performed with 5 µM Zinpyr-1 in a solution of HBSS buffer at 37 °C for 30 min. To reach 5 µM, 10 µL of a 1 mM Zinpyr-1 stock solution in sterile ATCC Dimethylsulfoxide (DMSO) 5×5 was added to the dish containing cells in 2 mL HBSS. The resulting solution contains less than 0.5% DMSO. After incubation, cells were washed with warm HBSS and 2 mL of HBSS was added before imaging. Images were collected using a Nikon DS-Qi1 Quantitative Monochrome Digital Camera with a 20× objective. The filter used for imaging Zinpyr-1 fluorescence was a B-2E/C FITC Cube with an excitation range of λ=465-495 nm and emission range of λ=515-555 nm. Photocage solutions added during these imaging experiments were added at 25 µM increments and images were obtained a minimum of 2 min after addition of each component. The stock solutions used to make the photocage complexes were 40 mM stock solutions of the photocage (ligand only) dissolved in sterile ATCC Dimethylsulfoxide (DMSO), 20 mM stock of $ZnCl_2$ in millipore water, and 20 mM stock of pyrithione in DMSO. Final solutions of the tested cages with varying components were made in millipore water with 10% DMSO. Solutions were made fresh before each imaging experiment. The ternary complexes were made to a final concentration of 1.38 mM (20 µL cage stock, 10 µL $ZnCl_2$ stock, 9 µL pyrithione stock, 251 µL Millipore water), and the complexes that did not contain ionophore were made to a final concentration of 2 mM (20 µL cage stock, 10 µL $ZnCl_2$ stock, 170 µL Millipore water). These stock solutions were added to the culture dish containing cells and 2 mL of HBSS to a final concentration of 25 µM. TPEN was added at the end of each experiment from a 5 mM stock solution in DMSO. ZTRS labeling was performed with 5 µM ZTRS in a solution of HBSS buffer at 37 °C for 30 min. To reach 5 µM, 10 µL of a 1 mM ZTRS stock solution in sterile ATCC Dimethylsulfoxide (DMSO) was added to dish containing cells in 2 mL HBSS. After incubation, cells were washed with warm HBSS and 2 mL of HBSS was added before imaging as described above. Photocage solutions used in ZTRS photolysis experiments were prepared as previously described for the Zinpyr-1 experiments. Photolysis was performed with the shutter light of the microscope (λ_{ex} = 330-380 nm) through the UV-2A filter. To evaluate the cell images semi-quantitatively, corrected total cell fluorescence (CTCF, which equals the integrated density after subtracting the product of the area of selected cell and the mean background fluorescence) as measured using ImageJ software[19] The CTCF value allows for a comparison of the cell fluorescence that results from the changing experimental conditions. Control imaging studies with Zinpyr-1 (Figure S32-S34) can be found in the supporting information.

RT-PCR Assays with ZnT-1 and MT-2. A 20 mM stock solution of photocage in sterile DMSO, and 40 mM solution of both pyrithione and $ZnCl_2$ were prepared in Millipore water. [Zn(DPAdeCage)(pyrithione)] and [Zn(XDPAdeCage)(pyrithione)] solutions were prepared by mixing 1 equivalent photocage, 1 equivalent $ZnCl_2$, and 0.9 equivalents pyrithione in Millipore water (pH 7.5) to a final concentration of 1 mM. A control solution was prepared by mixing Millipore water and DMSO to same ratio as the cage solutions. A 1 mM [Zn(pyrithione)$_2$] solution was prepared in Millipore water and DMSO.

Once the cells reached confluency, the plates were covered in aluminum foil, and a different solutions was added to each of the wells that also contained 2 mL fresh DMEM media. The volume added to each well was 50 µL to reach 25 µM (0.5% final percentage DMSO). All dishes incubated 3 min after addition of photocage, control, or Zn^{2+} solution. After incubation all wells were washed with PBS, and 2 mL fresh DMEM was added to each. For the light exposed dishes, 365 nm UV light was directed onto the samples for 1 minute. All other dishes were kept in the dark. Following an additional 10 min incubation time, the cells were trypsinized, pelleted, and frozen.

Isolation and purification of RNA from the frozen cell pellets of the cultured cells was completed using Qiagen RNeasy Mini Kit according to the manufacturer's protocol. Synthesis of cDNA from purified RNA was completed using Thermo Scientific RevertAid First Strand cDNA Synthesis according to the manufacturer's protocol. RT-PCR was performed with the LightCycler® 96 Instrument. The sequences of the primers used for RT-PCR obtained from Sigma Aldrich.[20-22] The relative quantity $e^{-\Delta CT}$ (CT: cycle threshold) of ZnT-1 and MT-2 was calculated using the internal control gene GAPDH,[23] where ΔCT = ($CT_{\text{gene of interest}}$ - $CT_{\text{internal control}}$). RT-PCR primer sequences are provided in the supporting information.

RESULTS AND DISCUSSION

Ligand design, synthesis and metal binding properties. Benzophenone derivatives such as 2-xanthone acetic acid (XAA) undergo photodecarboxylation similarly to *m*NPAs, but with higher ε at longer λ_{max}.[14, 24] The XAA ketone and *m*NPA nitro-groups provide the pathway to the excited state necessary for carbanion formation. To test the hypothesis that XAA was suitable for Zn^{2+} photocages, we designed a photocage utilizing a DPA-based (dipicolyl amine) ligand. The DPA receptor was targeted specifically to prevent ligand exchange reactions of Zn^{2+} complexes with alkaline earth metal ions as observed with NTAdeCage. Substituting softer pyridyl donors for hard carboxylate ligands eliminates Mg^{2+} and Ca^{2+} displacement of photocage-coordinated Zn^{2+}.

Scheme 1. (A) Synthesis of XDPAdeCage and (B) DPAdeCage

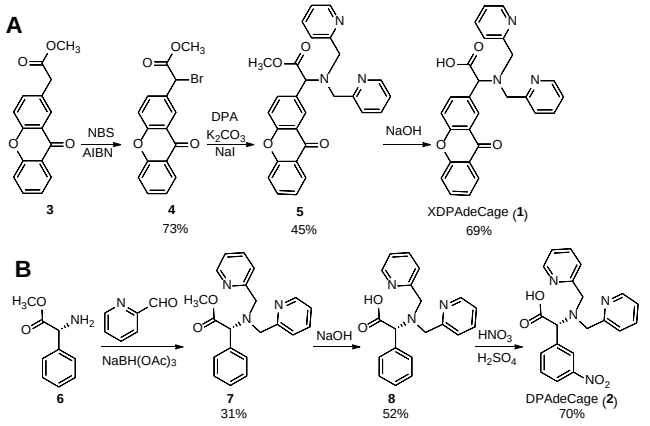

XDPAdeCage (**1**, XDPA *X*anthone–*DPA de*carboxylation photo*Cage*) was prepared using a modular three-step synthesis starting from compound (**3**).[14] Compound **3** was brominated analogously to other xanthone derivatives.[25] Following nucleophilic displacement by DPA and saponification, XDPAdeCage was obtained in 23% overall yield (Scheme 1A). We anticipate this new synthetic approach will be amenable to constructing a variety of photocages with metal ion binding properties tuned for specific applications.

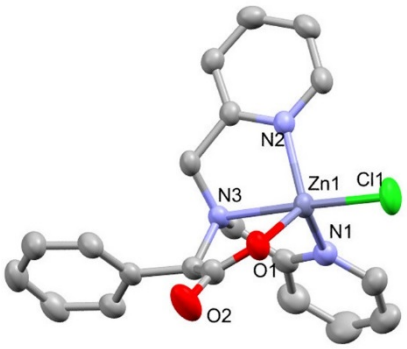

Figure 2. Thermal ellipsoid representation of [Zn(**8**)Cl] at the 50% probability level and selected atom labels. Selected bond distances (Å) and bond angles (°) can be found in Table 2.

In order to compare the optical properties of the XAA and *m*NPA photocaging groups, we also prepared the analogous *m*NPA-based photocage DPAdeCage (**2**). Direct comparison of XDPAdeCage and NTAdeCage would not adequately account for the impact of the pendant donor groups on the photochemistry. Pyridine rings in particular have low-lying excited states,[26] and can provide deactivation channels for excited chromophore. DPAdeCage was prepared in 11% overall yield using the synthesis used to access NTAdeCage except reductive amination with 2-pyridine carboxaldehyde was used to alkylate the amino group (Scheme 1B). Unlike XDPAdeCage, which is derived from a non-stereospecific free radical bromination reaction, the DPAdeCage starts with an enantiomerically pure amino acid derivative. Although XDPAdeCage is isolated as a racemate, we do not predict any impact on the other photocaging properties.

The expected coordination behavior of the DPA-carboxylate receptor was confirmed using the photocage structural analog **8** that was crystallized with $ZnCl_2$ (Figure 2). The [Zn(**8**)Cl] complex adopts a slightly distorted trigonal bipyramid (τ = 0.87) with the aliphatic amine ligand and chloride occupying the axial positions. Since XDPAdeCage and **8** share the same receptor, we expect a nearly identical coordination geometry regardless of the pendant aryl group. The control photocage DPAdeCage also should bind Zn^{2+} identically. The formation of a discrete 1:1 complex is apparent in ^{1}H NMR titrations where ligand peaks of XDPAdeCage gradually erode with the concomitant appearance of complex peaks corresponding to $[Zn(XDPAdeCage)]^+$. Similar to changes were observed in NMR titration experiments showing the formation of the $[Zn(NTAdeCage)]^{1-}$ complex.[13] In addition to NMR titrations and X-ray structures, the [Zn(**8**)Cl] complex was observed at m/z = 432.04 in the HRMS spectrum, which suggests the complex is relatively robust.

Scheme 2. Uncaging of $[Zn(XDPAdeCage)]^+$ (A) and $[Zn(DPAdeCage)]^+$ (B)

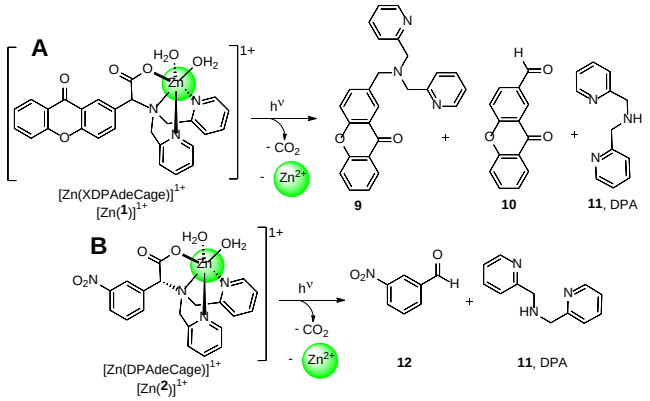

The Zn^{2+} binding properties of XDPAdeCage were assessed by competitive ligand exchange with 4-(2-pyridylazo) resorcinol (PAR). The erosion of the distinctive absorption bands associated with the $[Zn(PAR)_2]$ complex upon extraction of Zn^{2+} by another chelator provide a convenient spectroscopic handle to interrogate metal ion binding. The titrations in triplicate with $[Zn(PAR)_2]$ reveal that XDPAdeCage conforms to the 1:1 Zn^{2+}:ligand binding mode observed in the NMR titrations and crystal structure. Under simulated physiological conditions (40 mM HEPES, pH 7.0, 100 mM KCl), XDPAdeCage exhibits a K_d of 4.6±0.8 pM. Since the DPA photoproduct has K_d of 160 nM, the ΔK_d will be 3.3×10^4.

In comparison with NTAdeCage (0.10 pM K_d; 6.3×10^4 ΔK_d), XDPAdeCage has a slightly diminished Zn^{2+} buffering capacity and ability to shift the binding equilibrium upon photolysis. The loss of binding affinity is analogous to the differences in carboxylate-rich EDTA (0.032 fM K_d,

ethylenediaminetetraacetic acid) and pyridine-rich TPEN (0.25 fM, tetra(pyridyl)ethylenediamine) due in part to electrostatic effects. Importantly however, neither Ca^{2+} nor Mg^{2+} showed any measurable Zn^{2+}-binding interference with XDPAdeCage, which is also consistent with the selectivity of TPEN for Zn^{2+} over Ca^{2+} and Mg^{2+}. In complex biological milieu a significant increase in specificity readily offsets any slight loss of affinity. As we have demonstrated previously,[11] insufficient metal binding equilibria can be compensated for by increasing the ratio of photocage to Zn^{2+} in solution.

DPAdeCage has an order of magnitude stronger binding (0.8±0.3 pM) and therefore a slightly higher ΔK_d (2.0×10^5) than XDPAdeCage, but otherwise identical metal ion binding properties. While there is no obvious reason to expect DPAdeCage to bind Zn^{2+} more tightly, the larger xanthone ring may introduce some steric constraints or electrostatic diffences that impact the stability of the resulting metal complex. In non-biological systems that are less susceptible to photodamage, the slightly improved Zn^{2+} binding properties may prove advantageous.

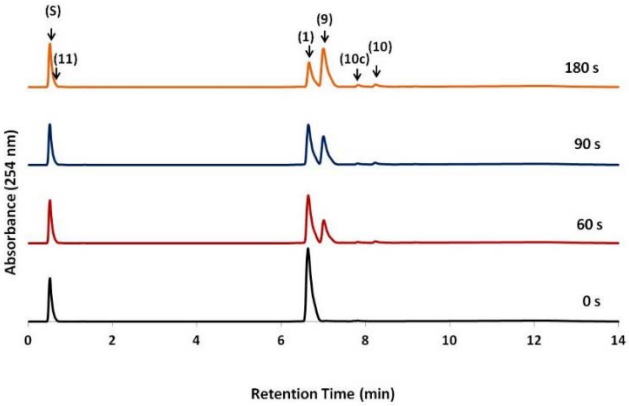

Figure 3. HPLC stack plot showing the photolysis of 0.975 mM $[Zn(XDPAdeCage)]^{1+}$ (pH 7.5, 50% CH_3OH) at 60, 90, and 180 s (365 nm). Isonicotinic acid (0.2 M, CH_3OH) was used as internal standard (**S**). Photoproducts are labeled as **9**, **10**, **10c** (a trace putative aldehyde coupling product, Scheme S1) and **11.** Only apo-chelators including XDPAdeCage (**1**) and **11** are detected by MS indicating decomplexation on the LC column.

Photodecarboxylation and demonstration of Zn^{2+} release. The photoreactivity of apo-XDPAdeCage and $[Zn(XDPAdeCage)]^+$ was assessed by LC-MS using UV light irradiation (Scheme 2A, 365 nm). After irradiating either the apo-photocage or the Zn^{2+} complex for 120 s (40 mM HEPES, 100 mM KCl, pH 7.5, 50% CH_3CN), three new peaks appeared in the LC trace (Figure 3) corresponding to the decarboxylated photoproduct (**9**, m/z = 408.2), a xanthone aldehyde (**10**, m/z = 225.1) and DPA (**11**, m/z = 200.1). After extended photolysis times (6 min), trace amounts of coupled products from radical reactions began to appear. By monitoring the disappearance of apo-XDPAdeCage and $[Zn(XDPAdeCage)]^+$, the $\Phi_{photolysis}$ was calculated as 20% and 27% respectively. Photolysis was performed in mixed solvent to retain photocage solubility at concentrations sufficient for UV-vis detection. Although the ratio of photoproducts varies somewhat depending on the nature of the co-solvent, decarboxylation occurs to give DPA-based photoproducts with identical Zn^{2+}-buffering capacities.

Unlike XDPAdeCage which has a clearly defined band at 347 nm (ε = 4730 $M^{-1}\cdot cm^{-1}$), the absorption spectrum of apo-DPAdeCage and $[Zn(DPAdeCage)]^+$ closely resemble that of NTAdeCage where the λ_{max} for the *m*NPA group appears at 262 nm (Figure 4). The photolysis of *m*NPA-derived photocages relies on photons absorbed by the weak tail above 300 nm when using standard uncaging wavelengths (ca. 350 nm). Interestingly, $[Zn(DPAdeCage)]^+$ has an even weaker absorbance above 300 nm than NTAdeCage. Near UV light is typically required for nitrobenzyl photocages to break C–C or C–H bonds. Unlike nitrobenzyl groups that have poor two-photon cross sections, xanthone groups are often amenable to multi-photon techniques,[27] and will be the subject of future investigations.

The photoproducts observed upon uncaging of both apo-DPAdeCage and $[Zn(DPAdeCage)]^+$ are similar to the XDPAdeCage counterparts (Scheme 2B). Irradiating a solution apo-DPAdeCage or the Zn^{2+} complex (40 mM HEPES, 100 mM KCl, pH 7.5, 20% CH_3OH) resulted in the appearance of *m*-nitrobenzaldehyde (GC-MS, m/z = 151) and DPA (m/z = 200.1,) with a concurrent decrease in apo-DPAdeCage (Figure 5). The $\Phi_{photolysis}$ were calculated as 40% and 5% for apo-DPAdeCage and $[Zn(DPAdeCage)]^+$ respectively. Unlike NTAdeCage, DPAdeCage exhibited a noticeable decrease in $\Phi_{photolysis}$ upon complexation. While the basis for this reduced photolysis efficiency is unclear, the absorbance above 300 nm is much weaker than that of NTAdeCage. We also hypothesize the difference in net charge at the Zn^{2+}-binding site affects the carbanion formation. During DPAdeCage photolysis, the formation of 3-nitrobenzaldehyde increases absorbance above 300 nm, which may facilitate DPAdeCage photolysis by an energy transfer mechanism.

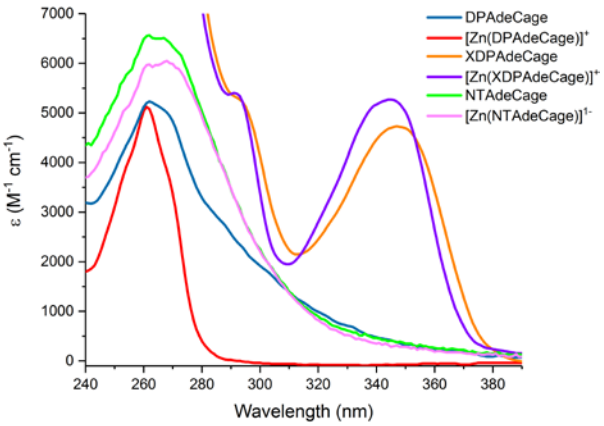

Figure 4. Absorption spectra of XDPAdeCage and $[Zn(XDPAdeCage)]^+$ (pH 7.5, 40 mM HEPES, 100 mM KCl, 10% CH_3CN); DPAdeCage and $[Zn(DPAdeCage)]^+$ (pH 7.5, 40 mM HEPES, 100 mM KCl, 10% CH_3OH); and NTAdeCage and $[Zn(NTAdeCage)]^{1-}$ (pH 7.5, 40 mM HEPES, 100 mM KCl). Extinction coefficients: XDPAdeCage, 4730 $M^{-1}\cdot cm^{-1}$ (λ_{347}); $[Zn(XDPAdeCage)]^+$, 5270 $M^{-1}\cdot cm^{-1}$ (λ_{344}); DPAdeCage, 5120 $M^{-1}\cdot cm^{-1}$ (λ_{261}); $[Zn(DPAdeCage)]^+$, 5230 $M^{-1}\cdot cm^{-1}$ (λ_{262}); NTAdeCage, 6562 $M^{-1}\cdot cm^{-1}$ (λ_{262}); $[Zn(NTAdeCage)]^+$, 5975 $M^{-1}\cdot cm^{-1}$ (λ_{262}). None of the mNPA photocages have an ε above 300 $M^{-1}\cdot cm^{-1}$ at the instrumental photolysis λ_{max} (λ_{365}), a wavelength typically employed in photocaging applications. The strong absorbance above 280 nm in the XDPAdeCage traces, which is characteristic of XAA derivatives, is truncated for clarity.

Regardless of reason, the less efficient uncaging limits the utility of DPAdeCage in biology despite the improved Zn^{2+}

binding properties. Of all the Zn^{2+} photocages prepared to date, only XDPAdeCage combines the red-shifted absorbance of a XAA chromophore with the enhanced Zn^{2+} specificity achieved with the DPA-based receptor. Furthermore, the $\Phi_{photolysis}$ of $[Zn(XDPAdeCage)]^+$ matches that of $[Zn(NTAdeCage)]^-$ within experimental error, which was previously the highest value measured for a Zn^{2+} photocage.

To demonstrate uncaging preliminarily, $[Zn(XDPAdeCage)]^+$ and $[Zn(DPAdeCage)]^+$ were photolyzed, and the release of Zn^{2+} was monitored by fluorescence spectroscopy using ZTRS, a Zn^{2+}-specific fluorescent sensor with an affinity between that of the intact photocaged complexes and photoproducts (5.7 nM K_d).[28] ZTRS has a weak emission (512 nm λ_{max}) that increases as photolysis proceeds and $[Zn(ZTRS)]^{2+}$ forms. As both photocaged complexes are irradiated, the fluorescence intensity at λ_{512} increases, although the emission plateaus more rapidly with $[Zn(XDPAdeCage)]^+$ than $[Zn(DPAdeCage)]^+$, which is consistent with a more efficient photolysis of the XAA-derived photocage at the wavelengths used. Similarly, $[Zn(PAR)_2]$ formation can be observed by monitoring absorbance at λ_{550} over the course of the photolysis of either complex. These results are consistent with the more tightly binding photocages sequestering Zn^{2+} until the photolysis forms more weakly binding photoproducts that readily undergo ligand exchange with the competing chelators.

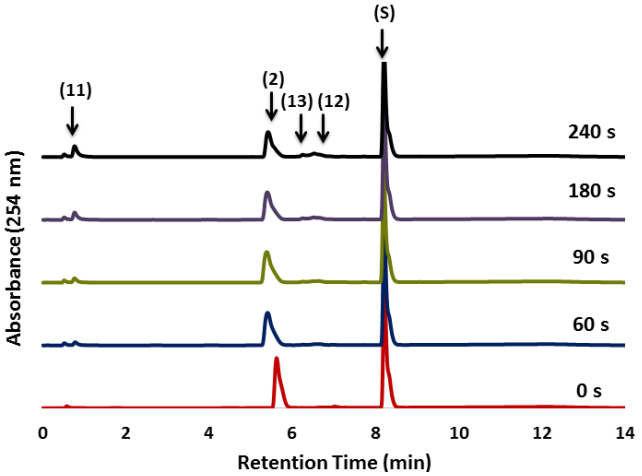

Figure 5. HPLC stack plot showing the photolysis of 1.95 mM $[Zn(DPAdeCage)]^{1+}$ (pH 7.5, 40 mM HEPES, 100 mM KCl, 20% CH_3OH) at 60, 90, 180, and 240 s (365 nm). Isonicotinic acid (0.2 M, CH_3OH) was used as internal standard (**S**). Photoproducts are labeled as **11**, **12** and **13** (a trace putative ketone, Scheme S2). Only apo-chelators including DPAdeCage (**2**) and **11** are detected by MS indicating decomplexation on the LC column.

Demonstration of intracellular Zn^{2+} release with fluorescence imaging and protein expression. When interrogating intracellular Ca^{2+}, apo-photocages typically are introduced and allowed to acquire free Ca^{2+} from the cytoplasm.[9] After intracellular equilibrium is reestablished, the photocaged complexes can be photolyzed to initiate Ca^{2+} signals. Since intracellular Zn^{2+} is tightly bound to critical proteins, introducing strong Zn^{2+} chelators can negatively impact cell viability.[29] When metallated, ZinCleav, NTAdeCage and both the new photocages are charged species, which limits the photocaged complexes propensity to cross lipophilic membranes. To avoid invasive techniques like microinjection that could perturb cellular function, we hypothesized that neutralizing the charge of $[Zn(XDPAdeCage)]^+$ by forming a ternary complex with an anionic ligand would allow the photocaged complexes to cross cellular membranes passively.

To test this hypothesis, we labeled human dermal fibroblast (HDF) cells with the cell-permeant fluorescent probe ZP1,[30] and treated the cells with a solution of [Zn(XDPAdeCage)(pyrithione)] generated *in situ*. The treatment led to an increase in perinuclear ZP1 emission similar to reported imaging studies using $[Zn(pyrithione)_2]$, which transports Zn^{2+} across cellular membranes, and was reversible upon treatment with TPEN. This result is consistent with an intracellular ligand exchange reaction between the weaker binding XDPAdeCage ligand and the stronger binding ZP1 fluorescent sensor (0.04 pM K_d). Additional control studies conducted with $[Zn(XDPAdeCage)]^+$ in the absence of pyrithione showed no increase in ZP1 emission. Analogous experiments with $[Zn(DPAdeCage)]^+$ and the photostable $[Zn(\mathbf{8})]^+$ model complex in the presence and absence of pyrithione produced similar results.

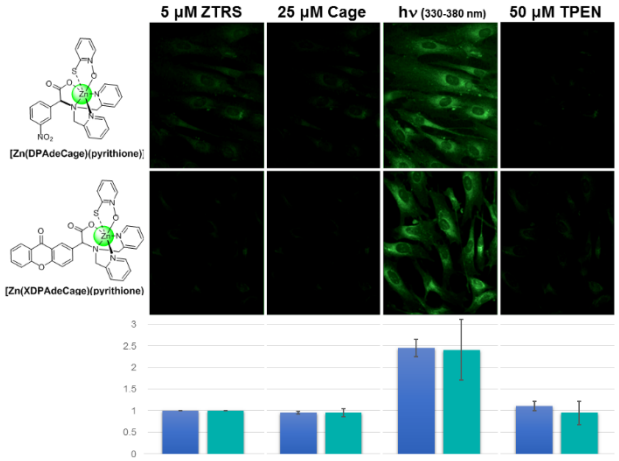

Figure 6. Imaging of Zn^{2+} uncaging using fluorescence microscopy**.** HDF cells were labeled with 5 μM ZTRS, and intracellular emission response was quantified using fluorescence microscopy. Emission does not increase following addition of [Zn(DPAdeCage)(pyrithione)] (top) or [Zn(XDPAdeCage)(pyrithione)] (bottom), but after exposure to the microscope light source through a UV-range filter at 5 s increments, the intracellular emission increases. Total cell fluorescence increases 2.5-fold over 120 s, and the response is reversed by TPEN addition. The average corrected total cell fluorescence (CTCF) was calculated over three trials. The blue and green bars correspond to the CTCF experiments with $[Zn(XDPAdeCage)]^+$ and $[Zn(DPAdeCage)]^+$ respectively.

Adding pyrithione does not appear to impact the photolysis of $[Zn(XDPAdeCage)]^+$ and $[Zn(DPAdeCage)]^+$; however, the association constant is probably weaker than the log K of $[Zn(pyrithione)]^{1-}$, which is only 5.1.[31] A 4-fold excess of pyrithione was used to effectively shift the binding equilibrium toward the ternary complex to conduct *in vitro* photolysis experiments, but these conditions are not directly reflective of those in the cellular assays. The formation of the ternary complex is therefore best envisaged as an equilibrium process that allows passage of the photocage across cellular membranes, but not necessarily one that leads to a persistent intracellular Zn^{2+} ternary complex.

When labeled with ZTRS instead of ZP1 (Figure 6), treatment with [Zn(XDPAdeCage)(pyrithione)] led to minimal changes in intracellular emission until the cells were exposed to the microscope light source (330–380 nm λ). Over 120 s, ZTRS emission gradually plateaus, and the response is reversible upon TPEN addition. The results are consistent with only ternary pyrithione complexes diffusing across the cellular membrane, and photolysis of the light-sensitive chelators increasing Zn^{2+} availability to the ZTRS sensor. The intracellular fluorescence response of ZTRS upon uncaging is identical to the benchtop assays except the [Zn(DPAdeCage)(pyrithione)] provides an emission response on a timescale similar to [Zn(XDPAdeCage)(pyrithione)]. The apparent improvement in $[Zn(DPAdeCage)]^+$ photolysis in cells may indicate indirect photocage excitation pathways involving energy transfer from endogenous light-absorbing chromophores, or other impacts of the intracellular environment on the photocage. This phenomenon will be explored further as a potential avenue to expanding the use of *m*NPA-based photocages.

We obtained further evidence that Zn^{2+} delivery with XDPAdeCage elicits a cellular response using RT-PCR techniques to measure expression levels of metallothioneins (MT) and zinc transporters (Figure 7, ZnT).[20] MTs help maintain homeostasis by trapping excess cytosolic Zn^{2+},[32] and ZnTs remove Zn^{2+} from the cytosol through both efflux from the cell and sequestration into subcellular compartments;[33] therefore, any increase in cytosolic Zn^{2+} should be accompanied by increases in MT and ZnT expression. After loading HDF cells with [Zn(XDPAdeCage)(pyrithione)] and irradiating for 60 s, a nearly 3-fold increase in MT expression was measured using the RT-PCR primers to amplify the corresponding gene compared to the photocage-free control assay. In addition, treating cells with [Zn(XDPAdeCage)(pyrithione)] without subjecting the cells to photolysis conditions resulted in negligible changes in gene expression. Analogous experiments with ZnT primers resulted in a 6-fold increase in protein expression. Nearly identical increases in ZnT and MT expression were measured when using the labile $[Zn(pyrithione)_2]$ complex to increase cytosolic Zn^{2+} levels in a light-independent manner as previously demonstrated.[20, 22, 34-35]

Experiments conducted in parallel with DPAdeCage also exhibited increases in ZnT and MT expression in cells exposed to light compared to those kept in the dark. In comparison to XDPAdeCage however, the absolute change in expressed in the light-free and light-exposed cells was somewhat smaller, which suggests a less efficient Zn^{2+} delivery. The cumulative results with the photocages, and accompanying control experiments indicate that both DPAdeCage and XDPAdeCage can transport Zn^{2+} across the cellular membrane as ternary complexes with pyrithione, and release Zn^{2+} upon photolysis. In response to the photoinduced discharge of Zn^{2+}, cells maintain homeostasis by increasing the expression of regulatory proteins. Neither photocage perturbs the Zn^{2+} trafficking machinery of the cell in the absence of light however.

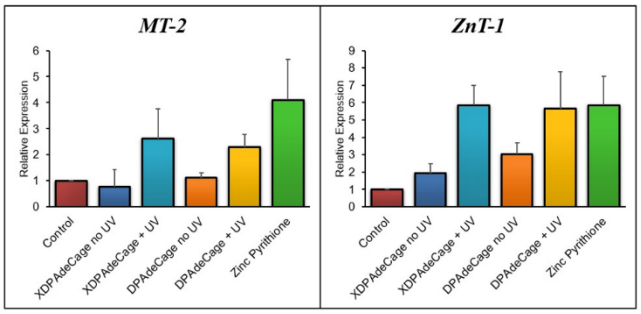

Figure 7. Relative expression of Zn^{2+}-responsive genes in HDF cells. RT-PCR was performed on the cDNA derived from HDF cells exposed treated with different complexes and light exposure. Control cells were given no photocage or Zn^{2+}. Photocage treated cells were either incubated with 25 μM [Zn(XDPAdeCage)(pyrithione)] or [Zn(DPAdeCage)(pyrithione)], and then either kept in the dark or exposed to 365 nm light. As a positive control, cells were incubated with 25 μM $[Zn(pyrithione)_2]$. The relative quantity of *ZnT-1* and *MT-2* was calculated using the housekeeping gene GAPDH. The relative value of these genes expressed in the control cDNA was normalized to 1. Error bars represent the variation over three separate RNA isolations.

CONCLUSIONS

Many questions remain about the signaling functions of Zn^{2+} in the central nervous system; however, better photochemical tools are necessary to conduct the kinds of experiments to delineate the various pathways. XDPAdeCage represents a significant improvement over the previous generations of photocaged complexes for Zn^{2+} owing to improved optical properties and uncaging efficiency. Furthermore, the demonstration that impermeant photocaged complexes can be converted into a permeant ones by assembly of ternary complexes, provides a roadmap to reducing the molecular engineering to synthesize photocaged complexes with all the necessary features for implementation in cells. The XDPAdeCage can either be used as an extracellular photocage, or to probe intracellular processes, depending on the absence or presence of pyrithione. The successful proof of concept fluorescence imaging studies and light-mediated control of protein expression are the precursor experiments to a broader exploration of Zn^{2+} signaling process with XDPAdeCage and related photocaged complexes.

Table 1. Crystallographic Parameters for [Zn(**8**)]Cl

formula	$C_{20}H_{18}Cl_1N_3O_2$
formula wt (M_r)	433.21
Crystal system, space group	Triclinic, *P*-1
a, Å	8.8076(11)
b, Å	9.6808(13)
c, Å	11.8655(17)
α, °	79.574(6)
β, °	69.967(6)
γ, °	75.363(7)
V, Å^3	914.7(2)
Z	2
ρ_{calcd} (g cm^{-3})	1.573

absorp. coeff. μ (mm^{-1})	1.509
temp, K	296
total no. data	7244
no. unique data	3238
obs. data[a]	2917
R, %[b]	0.0250
wR2, %[c]	0.0637
no. of parameters	244
max/min peaks, e/Å	0.57/-0.24

[a] Observation criterion: $I > 2\sigma(1)$. [b] $R = \Sigma ||F_o| - |F_c|| / \Sigma |F_o|$. [c] $wR2 = [\Sigma (w (F_o^2 - F_c^2)^2) / \Sigma w(F_o^2)^2]^{1/2}$.

Table 2. Selected Interatomic Distances (Å) and Angles (deg) for [Zn(**8**)]Cl

bond length	bond angle
Zn–O(1) 1.989(2)	O(1)–Zn–N(1) 115.63(7)
Zn–Cl(1) 2.267(6)	O(1)–Zn–N(2) 121.15(6)
Zn–N(1) 2.096(2)	N(1)–Zn–N(2) 108.77(7)
Zn–N(2) 2.079(2)	Cl(1)–Zn–N(3) 177.20(5)
Zn–N(3) 2.287(1)	N(1)–Zn–N(3) 76.69(6)
	Cl(1)–Zn–N(2) 103.81(5)
	O(1)–Zn–N(3) 77.49(6)

ASSOCIATED CONTENT

Supporting Information

Experimental procedures for routine metal binding and photochemistry assays. RT-PCR primer sequences. Schemes for the proposed photolysis mechanisms of XDPAdeCage (S1) and DPAdeCage (S2). Figures for additional LC traces under different conditions for XDPAdeCage (S1-S7) and DPAdeCage (S23) photolysis. Figures for UV-vis and emission spectra under different conditions for XDPAdeCage (S8-S18) and DPAdeCage (S24-S27 and S29) photolysis. Figures for the UV-vis for [Zn(XDPAdeCage)(pyrithione)] S19-S20 and [Zn(DPAdeCage)(pyrithione)] (S28 and S31) phtolysis. Figures for UV-vis spectra of Ca^{2+} and Mg^{2+} competitions studies for XDPAdeCage (S21-S22) and DPAdeCage (S30). Figures for additional cellular fluorescence imaging (S32-34). Figures for NMR spectra of XDPAdeCage titration with Zn^{2+} (S35) and photolysis (S36). Figures for NMR spectra of all new compounds (S37-S50). Figure for MS spectra of new compounds and [Zn(**8**)Cl] (S51). Figure for fully labeled thermal ellipsoid representation of [Zn(**8**)Cl] (S52). Tables of additional X-ray data (S1-S5).

AUTHOR INFORMATION

Corresponding Author

*scburdette@wpi.edu

ORCID

Shawn C. Burdette: 0000-0002-2176-0776

Notes

The authors declare no competing financial interests.

ACKNOWLEDGMENT

We thank Christopher Lambert for assistance with HDF cells. This work was supported by NSF Grant CHE-0955361.

REFERENCES

(1) Chabosseau, P.; Woodier, J.; Cheung, R.; Rutter, G. A., Sensors for measuring subcellular zinc pools. *Metallomics* **2018,** *10* (2), 229-239.
(2) Barr, Chelsea A.; Burdette, Shawn C., The zinc paradigm for metalloneurochemistry. *Essays Biochem.* **2017,** *61* (2), 225-235.
(3) Pan, E.; Zhang, X.-a.; Huang, Z.; Krezel, A.; Zhao, M.; Tinberg, Christine E.; Lippard, Stephen J.; McNamara, James O., Vesicular Zinc Promotes Presynaptic and Inhibits Postsynaptic Long-Term Potentiation of Mossy Fiber-CA3 Synapse. *Neuron* **2011,** *71* (6), 1116-1126.
(4) Blakemore, L. J.; Tomat, E.; Lippard, S. J.; Trombley, P. Q., Zinc released from olfactory bulb glomeruli by patterned electrical stimulation of the olfactory nerve. *Metallomics* **2013,** *5* (3), 208-213.
(5) Khan, M.; Goldsmith, C. R.; Huang, Z.; Georgiou, J.; Luyben, T. T.; Roder, J. C.; Lippard, S. J.; Okamoto, K., Two-photon imaging of Zn^{2+} dynamics in mossy fiber boutons of adult hippocampal slices. *Proc. Nat. Acad. Sci. U.S.A.* **2014,** *111* (18), 6786-6791.
(6) Anderson, C. T.; Radford, R. J.; Zastrow, M. L.; Zhang, D. Y.; Apfel, U.-P.; Lippard, S. J.; Tzounopoulos, T., Modulation of extrasynaptic NMDA receptors by synaptic and tonic zinc. *Proc. Nat. Acad. Sci. U.S.A.* **2015,** *112* (20), E2705-E2714.
(7) Li, Y.; Andereggen, L.; Yuki, K.; Omura, K.; Yin, Y.; Gilbert, H.-Y.; Erdogan, B.; Asdourian, M. S.; Shrock, C.; de Lima, S.; Apfel, U.-P.; Zhuo, Y.; Hershfinkel, M.; Lippard, S. J.; Rosenberg, P. A.; Benowitz, L., Mobile zinc increases rapidly in the retina after optic nerve injury and regulates ganglion cell survival and optic nerve regeneration. *Proc. Nat. Acad. Sci. U.S.A.* **2017,** *114* (2), E209-E218.
(8) Gwizdala, C.; Burdette, S. C., Photo-release of Metal Ions in Living Cells. In *Inorganic Chemical Biology: Principles, Techniques and Applications*, Gasser, G., Ed. John Wiley and Sons Ltd: West Sussex, UK, 2014; pp 275-308.
(9) Ellis-Davies, G. C. R., Neurobiology with Caged Calcium. *Chem. Rev.* **2008,** *108* (5), 1603-1613.
(10) Gwizdala, C.; Singh, C. V.; Friss, T. R.; MacDonald, J. C.; Burdette, S. C., Quantifying factors that influence metal ion release in photocaged complexes using ZinCast derivatives. *Dalton Trans.* **2012,** *41* (26), 8162-8174.
(11) Bandara, H. M. D.; Kennedy, D. P.; Akin, E.; Incarvito, C. D.; Burdette, S. C., Photoinduced Release of Zn^{2+} with ZinCleav-1: a Nitrobenzyl-Based Caged Complex. *Inorg. Chem.* **2009,** *48* (17), 8445-8455.
(12) Bandara, H. M. D.; Walsh, T. P.; Burdette, S. C., A Second-Generation Photocage for Zn^{2+} Inspired by TPEN: Characterization and Insight into the Uncaging Quantum Yields of ZinCleav Chelators. *Chem. Eur. J.* **2011,** *17* (14), 3932-3941.
(13) Basa, P. N.; Antala, S.; Dempski, R. E.; Burdette, S. C., A Zinc(II) Photocage Based on a Decarboxylation Metal Ion Release Mechanism for Investigating Homeostasis and Biological Signaling. *Angew Chem.* **2015,** *127* (44), 13219-13223.
(14) Blake, J. A.; Lukeman, M.; Scaiano, J. C., Photolabile Protecting Groups Based on the Singlet State Photodecarboxylation of Xanthone Acetic Acid. *J. Am. Chem. Soc.* **2009,** *131* (11), 4127-4135.
(15) Sheldrick, G. M. *SADABS*, University of Göttingen: Göttingen, Germany, 1996.
(16) SAINT-Plus, version 6.02; Bruker Analytical X-ray System, Madison, WI, 1999.
(17) Sheldrick, G. M., Crystal structure refinement with SHELXL. *Acta Crystallogr. C* **2015,** *71* (Pt 1), 3-8.
(18) Burdette, S. C.; Walkup, G. K.; Spingler, B.; Tsien, R. Y.; Lippard, S. J., Fluorescent sensors for Zn^{2+} based on a fluorescein platform: synthesis, properties and intracellular distribution. *J. Am. Chem. Soc.* **2001,** *123* (32), 7831-7841.
(19) McCloy, R. A.; Rogers, S.; Caldon, C. E.; Lorca, T.; Castro, A.; Burgess, A., Partial inhibition of Cdk1 in G2 phase overrides the SAC and decouples mitotic events. *Cell Cycle* **2014,** *13* (9), 1400-1412.

(20) Shen, H.; Qin, H.; Guo, J., Cooperation of metallothionein and zinc transporters for regulating zinc homeostasis in human intestinal Caco-2 cells. *Nutr. Res.* **2008,** *28* (6), 406-413.
(21) Sullivan, V. K.; Cousins, R. J., Competitive reverse transcriptase–polymerase chain reaction shows that dietary zinc supplementation in humans increases monocyte metallothionein mRNA levels. *J. Nutr.* **1997,** *127* (5), 694-698.
(22) Zhao, W.-j.; Song, Q.; Wang, Y.-h.; Li, K.-j.; Mao, L.; Hu, X.; Lian, H.-z.; Zheng, W.-j.; Hua, Z.-c., Zn-responsive proteome profiling and time-dependent expression of proteins regulated by MTF-1 in A549 cells. *PloS One* **2014,** *9* (8), e105797.
(23) Schmittgen, T. D.; Livak, K. J., Analyzing real-time PCR data by the comparative C T method. *Nature Protoc.* **2008,** *3* (6), 1101.
(24) Blake, J. A.; Gagnon, E.; Lukeman, M.; Scaiano, J. C., Photodecarboxylation of Xanthone Acetic Acids: C−C Bond Heterolysis from the Singlet Excited State. *Org. Lett.* **2006,** *8* (6), 1057-1060.
(25) Rewcastle, G. W.; Atwell, G. J.; Baguley, B. C.; Boyd, M.; Thomsen, L. L.; Zhuang, L.; Denny, W. A., Potential antitumor agents. 63. Structure-activity relationships for side-chain analogs of the colon 38 active agent 9-oxo-9H-xanthene-4-acetic acid. *J. Med. Chem.* **1991,** *34* (9), 2864-2870.
(26) Cai, Z.-L.; Reimers, J. R., The Low-Lying Excited States of Pyridine. *J. Phys. Chem. A* **2000,** *104* (36), 8389-8408.
(27) Maity, D.; Sarkar, B.; Maiti, S.; Govindaraju, T., A Highly Selective Reaction-Based Two-Photon Probe for Copper(I) in Aqueous Media. *ChemPlusChem* **2013,** *78* (8), 785-788.
(28) Xu, Z.; Baek, K.-H.; Kim, H. N.; Cui, J.; Qian, X.; Spring, D. R.; Shin, I.; Yoon, J., Zn^{2+}-triggered amide tautomerization produces a highly Zn^{2+}-selective, cell-permeable, and ratiometric fluorescent sensor. *J. Am. Chem. Soc.* **2009,** *132* (2), 601-610.
(29) Ra, H.; Kim, H.-L.; Lee, H.-W.; Kim, Y.-H., Essential role of p53 in TPEN-induced neuronal apoptosis. *FEBS Lett.* **2009,** *583* (9), 1516-1520.
(30) Walkup, G. K.; Burdette, S. C.; Lippard, S. J.; Tsien, R. Y., A new cell-permeable fluorescent probe for Zn^{2+}. *J. Am. Chem. Soc.* **2000,** *122* (23), 5644-5645.
(31) Sun, P.-J.; Fernando, Q.; Freiser, H., Structure and Behavior of Organic Analytical Reagents. Formation Constants of Transition Metal Complexes of 2-Hydroxypyridine-1-Oxide and 2-Mercaptopyridine-1-Oxide. *Anal. Chem.* **1964,** *36* (13), 2485-2488.
(32) Krężel, A.; Maret, W., The Functions of Metamorphic Metallothioneins in Zinc and Copper Metabolism. *Int. J. Mol. Sci.* **2017,** *18* (6), 1237.
(33) Bafaro, E.; Liu, Y.; Xu, Y.; Dempski, R. E., The emerging role of zinc transporters in cellular homeostasis and cancer. *Signal Transduct. Target. Ther.* **2017,** *2*, 17029.
(34) Devergnas, S.; Chimienti, F.; Naud, N.; Pennequin, A.; Coquerel, Y.; Chantegrel, J.; Favier, A.; Seve, M., Differential regulation of zinc efflux transporters ZnT-1, ZnT-5 and ZnT-7 gene expression by zinc levels: a real-time RT–PCR study. *Biochem. Pharmacol.* **2004,** *68* (4), 699-709.
(35) Jayaraman, A. K.; Jayaraman, S., Increased level of exogenous zinc induces cytotoxicity and up-regulates the expression of the ZnT-1 zinc transporter gene in pancreatic cancer cells. *J. Nutr. Biochem.* **2011,** *22* (1), 79-88.

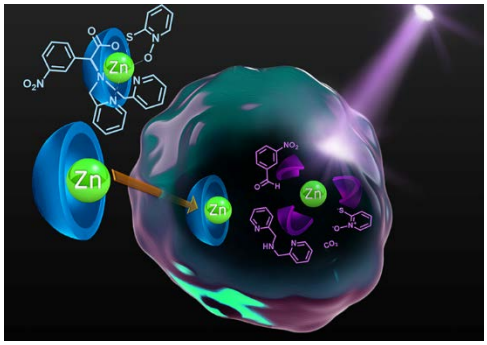
Zn
Zn
Zn
Zn